

Heat Capacity of a Strongly-Interacting Fermi Gas

J. Kinast, A. Turlapov, and J. E. Thomas*

Physics Department, Duke University, Durham, North Carolina 27708-0305

*To whom correspondence should be addressed; E-mail: jet@phy.duke.edu.

(Submitted 10 September, 2004)

We report on the measurement of the heat capacity for an optically-trapped, strongly-interacting Fermi gas of atoms. In the experiments, a precise input of energy to the gas is followed by single-parameter thermometry. The thermometry determines a temperature parameter \tilde{T} from the best fit of a Thomas-Fermi distribution with a fixed Fermi radius to the spatial density of the cloud. At $\tilde{T} = 0.33$, we observe a transition between two patterns of behavior: For $\tilde{T} = 0.33 - 2.15$, we find that the heat capacity closely corresponds to that of a trapped normal Fermi gas of atoms with increased mass. At low temperatures $\tilde{T} = 0.04 - 0.33$, the heat capacity clearly deviates from normal Fermi gas behavior.

Strongly-interacting, degenerate atomic Fermi gases (1) provide a paradigm for strong interactions in nature (2). Measurements of the interaction energy (1, 3, 4, 5) test predictions of universal interactions in nuclear matter (6, 7, 8), as well as effective field theories of strong interactions (9). The anisotropic expansion observed for strongly-interacting Fermi gases (1) is

analogous to the “elliptic flow” of a quark-gluon plasma (10). High temperature superfluidity has been predicted (11, 12, 13, 14, 15, 16, 17) in strongly-interacting Fermi gases, which can be used to test theories of high temperature superconductivity (18). Microscopic evidence for high temperature superfluidity has been obtained in the condensation of preformed pairs (19, 20) and in radio frequency measurements of the pairing gap (21, 22). Macroscopic evidence arises in anisotropic expansion (1) and in collective excitations (23, 24, 25).

In superconductivity and superfluidity, measurements of the heat capacity (26) have played an exceptionally important role in determining phase transitions (27) and in revealing the nature of the many-body quantum state of the system. We report on the measurement of the heat capacity for a strongly-interacting Fermi gas of ^6Li atoms, confined in an optical trap. Our experiments examine the fundamental thermodynamics of the gas. In the following, we first describe how the gas is prepared and our method for adding a precisely known energy to the gas. Then we discuss our technique of thermometry, which provides a monotonic temperature scale and a well-defined method for comparing experiment with predictions.

We prepare a degenerate 50-50 mixture of the two lowest spin states of ^6Li atoms by forced evaporation in an ultrastable CO_2 laser trap (28) as described previously (1). At a bias magnetic field of 840 G, just above the Feshbach resonance, the trap depth is lowered by a factor of $\simeq 580$ in a few seconds (1, 23) and then recompressed to 4.6% of the full trap depth in 1.0 s and held for 0.5 s to assure equilibrium. After a controlled amount of energy is added to the gas, as described below, the gas is allowed to thermalize for 0.1 s. Finally, the gas is released from the trap and imaged at 840 G to determine the number of atoms and the temperature parameter \tilde{T} . The column density is obtained by absorption imaging of the expanded cloud after 1 ms time of flight, using a two-level state-selective cycling transition (1, 23). In the measurements, we take optical saturation into account exactly and arrange to have very small optical pumping out of the two-level system. For our trap, the total number of atoms is $N = 2.2(0.3) \times 10^5$. From

the measured trap frequencies, corrected for anharmonicity, we obtain $\omega_{\perp} = \sqrt{\omega_x \omega_y} = 2\pi \times 1696(10)$ Hz and $\omega_z = 2\pi \times 72(5)$ Hz, so that $\bar{\omega} = (\omega_x \omega_y \omega_z)^{1/3} = 2\pi \times 592(14)$ Hz is the mean oscillation frequency. For these parameters, the typical Fermi temperature $T_F = (3N)^{1/3} \hbar \bar{\omega} / k_B$ for a noninteracting gas is $\simeq 2.5 \mu\text{K}$, small compared to the final trap depth of $U_0/k_B = 35 \mu\text{K}$.

Energy is precisely added to the trapped gas at fixed atom number by releasing the cloud from the trap and permitting it to expand for a short time t_{heat} after which the gas is recaptured. As shown below, even for the strongly-interacting gas, the energy input is well-defined for very low initial temperatures, where both the equation of state and the expansion dynamics are known. During the times t_{heat} used in the experiments, the axial size of the gas changes negligibly, while transverse dimensions expand by a factor $b_{\perp}(t_{\text{heat}})$. Hence, the harmonic trapping potential energy in each of the two transverse directions increases by a factor $b_{\perp}^2(t_{\text{heat}})$.

The initial potential energy is readily determined at zero temperature. This follows from the equation of state of the gas, $(1 + \beta)\epsilon_F(\mathbf{x}) + U_{\text{trap}}(\mathbf{x}) = \mu_0$ (I, 3, 29), where $\epsilon_F(\mathbf{x})$ is the local Fermi energy, β is the unitary gas parameter (I, 6, 3, 8, 30), U_{trap} is the harmonic approximation to the trapping potential, and μ_0 is the global chemical potential. The equation of state is equivalent to that of a harmonically trapped noninteracting gas of particles with an effective mass (7), which in our notation is $M^* = M/(1 + \beta)$, where M is the bare mass. Since the gas behaves as a harmonic oscillator, the mean potential energy is half of the total energy. As $\beta < 0$ (8), $M^* > M$, so that the effective oscillation frequencies and the chemical potential are simply scaled down, i.e., $\mu_0 = k_B T_F \sqrt{1 + \beta}$ (I, 3). The total energy at zero temperature, which determines the energy scale, is therefore

$$E_0 = \frac{3}{4} N \mu_0 = \frac{3}{4} N k_B T_F \sqrt{1 + \beta}. \quad (1)$$

For each direction, the initial potential energy at zero temperature is $E_0/6$. Then, the total

energy of the gas after heating is given by (31),

$$E(t_{heat}) = \eta E_0 \left[\frac{2}{3} + \frac{1}{3} b_{\perp}^2(t_{heat}) \right]. \quad (2)$$

Here, η is a correction factor arising from the finite temperature of the gas prior to the energy input. For the noninteracting gas, η_{nonint} is determined at the lowest temperature $\tilde{T} = 0.23$ from the energy for an ideal Fermi gas. For the strongly-interacting gas, where the initial temperature is very low and $\tilde{T} = 0.04$, we assume a Sommerfeld correction (32) and obtain $\eta_{int} \simeq 1 + 2\pi^2 \tilde{T}^2/3 \simeq 1.01$, which hardly affects the energy scale.

The strongly-interacting gas exhibits hydrodynamic, anisotropic expansion (1), so that $b_{\perp} = b_{\perp}^H$ is a hydrodynamic expansion factor (1, 33). For the noninteracting gas, we use a ballistic expansion factor $b_{\perp}^B(t) = \sqrt{1 + (\omega_{\perp} t)^2}$. The temperature change during the expansion time $t_{heat} \leq 460 \mu s$ must be very small, since the minimum value of $\tilde{T} = 0.04$ is measured by imaging the interacting cloud after 1 ms of expansion. Hence, the primary heating arises only after recapture and subsequent equilibration.

Thermometry of strongly interacting Fermi gases is not well understood. By contrast, thermometry of noninteracting Fermi gases can be simply accomplished by fitting the spatial distribution of the cloud with a Thomas-Fermi (T-F) profile, which is a function of two parameters. We choose them to be the Fermi radius σ_x and the reduced temperature T/T_F . However, this method is only precise at temperatures well below $0.5 T_F$, where σ_x and T/T_F are determined independently. At higher temperatures, where the Maxwell-Boltzmann limit is approached, such a fit determines only the product $\sigma_x^2 T/T_F$. We circumvent this problem by determining σ_x from a low temperature fit, and then hold it constant in the fits at all higher temperatures, enabling a one-parameter determination of the reduced temperature.

For strongly interacting Fermi gases below the superfluid transition temperature T_c , the spatial profile may contain normal and superfluid components (16). However, experimentally and

theoretically, one finds that the spatial profile of a strongly interacting gas closely resembles a T-F distribution (1, 34). For this reason, T-F fits to the cloud profiles are commonly used to estimate the reduced temperature, which is often reported as T/T_F , where T_F is the Fermi temperature for a noninteracting gas. Analogous to the noninteracting case, we define an experimental dimensionless temperature parameter \tilde{T} , which is to be determined by fitting the cloud profiles with a T-F distribution (35), holding constant the Fermi radius of the interacting gas, σ'_x . Unlike two parameter fitting procedures, this single parameter method is stable. We find experimentally that \tilde{T} increases monotonically from the highly degenerate regime to the Maxwell-Boltzmann limit. This fitting procedure also leads us to define a natural reduced temperature scale

$$\tilde{T}_{nat} \equiv \frac{k_B T}{\mu_0} = \frac{T}{T_F \sqrt{1 + \beta}}, \quad (3)$$

which is consistent with our choice of fixed Fermi radius σ'_x , i.e., $M\omega_x^2 \sigma_x'^2/2 = \mu_0$. At high temperatures, we must interpret $\tilde{T} = \tilde{T}_{nat}$, to obtain the correct Maxwell-Boltzmann limit. At low temperatures, $\tilde{T} \simeq \tilde{T}_{nat}$ yields an estimate of T/T_F . However, to determine the precise correspondence between \tilde{T} and the reduced temperature T/T_F which is input into theoretical models, one should perform the experimental fitting procedure with the theoretically generated density profiles as suggested and implemented by Chen et al., (36).

The experimental fitting procedure measures \tilde{T} by first obtaining one dimensional, transverse spatial distributions $n(x)$ from the column density by spatially integrating along the trap axial direction. Dividing by the total number of atoms per spin state, we obtain normalized spatial profiles. Then \tilde{T} is determined using the one parameter T-F fit method, yielding 0.04–2.15 for the strongly-interacting gas and 0.2–1.1 for the noninteracting gas.

The experimental energy scale Eq. 2 and the natural temperature scale Eq. 3 are determined by calculating β from the measured Fermi radii for the interacting and noninteracting gas samples. The relation is given by $\sigma'_x = \sigma_x(1 + \beta)^{1/4}$ (3), where $\sigma_x = \sqrt{2k_B T_F / (M\omega_x^2)}$

is the radius for a noninteracting gas. To determine σ'_x , we measure the size of the cloud after 1 ms of expansion, and scale it down by the known hydrodynamic expansion factor of $b_H(1 \text{ ms}) = 13.3$ (I, 33). We then determine the Fermi radius $\sigma'_x = 11.98 (N/2)^{1/6} \mu\text{m}/13.3 = 0.901(0.021) (N/2)^{1/6} \mu\text{m}$. Using $\sigma_x = 1.065 (N/2)^{1/6} \mu\text{m}$ for our trap parameters, yields $\beta = -0.49(0.04)$ (37) in reasonable agreement with the best current predictions, where $\beta = -0.56$ (8), and $\beta = -0.545$ (30).

We now apply our energy input and thermometry methods to measure the heat capacity of an optically trapped Fermi gas, i.e., for different values of t_{heat} , we measure the temperature parameter \tilde{T} and calculate the total energy $E(t_{\text{heat}})/E_0$ from Eq. 2. To obtain high resolution data, 30-40 different heating times t_{heat} are chosen. The data for each of these heating times are acquired in a random order to minimize systematic error. Ten complete runs are taken through the entire random sequence.

To test the method with a known system, we first measure the heat capacity for a noninteracting Fermi gas at 526 G. The gas is initially cooled to $\tilde{T} = 0.23$ (the lowest temperature we can achieve in this case) by 30 seconds of forced evaporation at 300 G as described previously (23), and then heated as described above. Fig. 1 shows the data (green dots) which represent the calculated $E(t_{\text{heat}})/E_0$ versus the measured value of \tilde{T} , for each t_{heat} . For comparison, predictions for a noninteracting, trapped Fermi gas, $E_{\text{ideal}}(\tilde{T})/E_{\text{ideal}}(0)$ are shown as the red curve, where $\tilde{T} = T/T_F$ in this case. Here, the chemical potential and energy are calculated using a finite temperature Fermi distribution and the density of states for the trapped gas. We use the density of states for a gaussian potential well (28), rather than the harmonic oscillator approximation. This yields very good agreement at all temperatures.

Next, we measure the heat capacity for the strongly interacting gas at 840 G. Here the gas is cooled to $\tilde{T} = 0.04$ and then heated. Fig. 1 shows the data (blue dots) which represent $E(t_{\text{heat}})/E_0$ versus the measured value of \tilde{T} , for each t_{heat} . Note that the temperature parameter

\tilde{T} varies by a factor of 50 and the total energy by a factor of 10. Remarkably, on a large scale plot, the data for the strongly interacting and noninteracting gases appear quite similar.

A striking result is shown by plotting the data for the strongly interacting gas on a $\log - \log$ scale. Fig. 2 shows that the data reveal a transition in behavior at $\tilde{T} \simeq 0.33$, where the slope changes. Above $\tilde{T} \simeq 0.33$, the data for strongly interacting data overlap closely with that of the noninteracting gas. Below $\tilde{T} \simeq 0.33$, the data deviates significantly from noninteracting Fermi gas behavior. This transition may arise from changes in the behavior of the total energy and from changes in the spatial profile of the gas which serves as our thermometer.

Insights into the microscopic structure of the strongly interacting gas can be obtained from the temperature scaling of the energy. Above the transition, for $\tilde{T} \geq 0.33$, we find that the data in Figures 1 and 2 are well fit by $E(\tilde{T}) = \sqrt{1+\beta} E_{ideal}(\tilde{T})$, with a constant $\beta = -0.49$. This suggests that $\tilde{T} = \tilde{T}_{nat} \equiv T/(T_F \sqrt{1+\beta})$ is a good approximation above the transition. Such scaling may be a manifestation of universal thermodynamics (38).

Below the transition, for $\tilde{T} \leq 0.33$, the gas may comprise several components, for example, a normal Fermi gas and both superfluid and noncondensed pairs, each contributing differently to the temperature scaling, as arises in a pseudogap model (16, 36). For simplicity, we consider here a temperature scaling of the form $E(\tilde{T})/E_0 = 1 + b \tilde{T}^c$. For sufficiently low temperature, one expects $c = 2$ for an ideal Fermi gas, $c = 5/2$ for a homogeneous noninteracting Bose gas, and $c = 4$ for a harmonically trapped Bose gas. The best fit (black line in Fig. 2) corresponds to $c = 2.53(0.15)$ and $b = 9.8(1.9)$. The χ^2 per degree of freedom for this fit is 1.4. We find that the parameters b and c are strongly correlated. Holding $c = 5/2$, we obtain $b = 9.4(0.2)$. Fitting a quadratic temperature dependence yields $b = 4.8(0.2)$, and a larger χ^2 per degree of freedom of 5.2. A T^4 power law fit yields $b = 63.8(4.1)$ and a χ^2 per degree of freedom of 7.1. These results suggest that the gas is neither a normal Fermi gas nor a BEC of small weakly interacting molecules.

One can understand $5/2$ power scaling at very low temperature as arising from thermal excitation of low energy bosons (fermion pairs) (18), where the fermionic contribution is exponentially suppressed by the superfluid gap. A simple picture of the $5/2$ power scaling is that short wavelength thermal excitations increase the local kinetic energy of bound pairs without breaking them, yielding the density of states and energy for free particles in three dimensions. To make an estimate of b based on universal scaling, we assume that the bosons have a mass of $2M^*$, so that the density of states per unit volume for a locally homogeneous gas is $(4M^*/\hbar^2)^{3/2}\epsilon^{1/2}/(4\pi^2)$. The total energy is easily determined using a Bose distribution with zero chemical potential. Assuming that the pairing energy scale is large compared to $k_B T$ over most of the trap volume, the ϵ integration is approximated from 0 to ∞ . Multiplying the resulting energy density by the trap volume N/\bar{n} , where \bar{n} is the average density, we obtain $E/E_0 = 1 + b\tilde{T}_{nat}^{5/2}$, where $b = (3/4)\zeta(5/2)(2\pi)^{3/2}(315/512) = 9.75$, close to the result $9.4(0.2)$ obtained from the fit.

We estimate the transition temperature from the intersection point, $\tilde{T} = 0.33(.02)$ (37), of the power law fit and the scaled ideal gas prediction, Fig. 2. To extract a preliminary value of T_c/T_F , we assume $\tilde{T} = \tilde{T}_{nat}$ near the transition temperature, and use the measured value of $\beta = -0.49$. We then obtain $T_c/T_F = \sqrt{1+\beta}\tilde{T} = 0.24(.02)$ (37), close to predictions for the superfluid transition temperature which have been made over the last decade (18, 39, 17, 40). The fractional change in the heat capacity C is estimated from the slope change in the fits to the data, assuming that the temperature calibration function is smooth near T_c (36). In that case, $(C_{>} - C_{<})/C_{>} = -0.48(0.03)$, where $> (<)$ denotes above (below) T_c .

Recently, Q. Chen, J. Stajic and K. Levin have done a pseudogap model of a trapped, strongly interacting Fermi gas (36), and obtain both the energy and the spatial profile as a function of reduced temperature T/T_F , throughout the superfluid and normal region. The temperature scale T/T_F is calibrated to our \tilde{T} by fitting one dimensional T-F profiles to the theoretical spatial distributions as described above, yielding a monotonic relation. The data of

Figures 1 and 2 are very well reproduced by the theory.

References and Notes

1. K. M. O'Hara, S. L. Hemmer, M. E. Gehm, S. R. Granade, J. E. Thomas, *Science* **298**, 2179 (2002).
2. M. E. Gehm, J. E. Thomas, *Am. Scientist* **92**, 238 (2004).
3. M. E. Gehm, S. L. Hemmer, S. R. Granade, K. M. O'Hara, J. E. Thomas, *Phys. Rev. A* **68**, 011401(R) (2003).
4. T. Bourdel, *et al.*, *Phys. Rev. Lett.* **93**, 050401 (2004).
5. M. Bartenstein, *et al.*, *Phys. Rev. Lett.* **92**, 120401 (2004).
6. H. Heiselberg, *Phys. Rev. A* **63**, 043606 (2001).
7. J. G. A. Baker, *Phys. Rev. C* **60**, 054311 (1999).
8. J. Carlson, S.-Y. Chang, V. R. Pandharipande, K. E. Schmidt, *Phys. Rev. Lett.* **91**, 050401 (2003).
9. J. V. Steele, Effective field theory power counting at finite density (2000). nucl-th/0010066.
10. P. F. Kolb, U. Heinz, *Quark Gluon Plasma 3* (World Scientific, 2003), p. 634. See Hydrodynamic Description of Ultrarelativistic Heavy Ion Collisions, arXiv: nucl-th/0305084.
11. M. Houbiers, *et al.*, *Phys. Rev. A* **56**, 4864 (1997).
12. R. Combescot, *Phys. Rev. Lett* **83**, 3766 (1999).

13. M. Holland, S. J. J. M. F. Kokkelmans, M. L. Chiofalo, R. Walser, *Phys. Rev. Lett.* **87**, 120406 (2001).
14. E. Timmermans, K. Furuya, P. W. Milonni, A. K. Kerman, *Phys. Lett. A* **285**, 228 (2001).
15. Y. Ohashi, A. Griffin, *Phys. Rev. Lett.* **89**, 130402 (2002).
16. J. Stajic, *et al.*, *Phys. Rev. A* **69**, 063610 (2004).
17. A. Perali, P. Pieri, L. Pisani, G. C. Strinati, *Phys. Rev. Lett.* **92**, 220404 (2004).
18. Q. Chen, J. Stajic, S. Tan, K. Levin, BCS-BEC crossover: From high temperature superconductors to ultracold superfluids (2004). ArXiv:cond-mat/0404274.
19. C. A. Regal, M. Greiner, D. S. Jin, *Phys. Rev. Lett.* **92**, 040403 (2004).
20. M. W. Zwierlein, *et al.*, *Phys. Rev. Lett.* **92**, 120403 (2004).
21. C. Chin, *et al.*, *Science* **305**, 1128 (2004).
22. M. Greiner, C. A. Regal, D. S. Jin, Probing the excitation spectrum of a fermi gas in the bcs-bec crossover regime (2004). ArXiv:cond-mat/0407381.
23. J. Kinast, S. L. Hemmer, M. E. Gehm, A. Turlapov, J. E. Thomas, *Phys. Rev. Lett.* **92**, 150402 (2004).
24. M. Bartenstein, *et al.*, *Phys. Rev. Lett.* **92**, 203201 (2004).
25. J. Kinast, A. Turlapov, J. E. Thomas, Breakdown of hydrodynamics in the radial breathing mode of a strongly-interacting fermi gas (2004). ArXiv:cond-mat/0408634; To appear in *Phys. Rev. A Rapid Comm.* **70**.
26. W. H. Keesom, K. Clusius, *Proc. Roy. Acad. (Amsterdam)* **35**, 307 (1932).

27. F. London, *Phys. Rev.* **54**, 947 (1938).
28. K. M. O'Hara, *et al.*, *Phys. Rev. Lett.* **82**, 4204 (1999).
29. This zero temperature equation of state for a unitary gas is supported by the observed spatial profiles at low temperatures, which are well approximated by a zero temperature T-F distribution as observed (1) and predicted (8, 30, 18). Further support arises from the measured radial breathing mode frequency at 840 G near resonance (25), which is in excellent agreement with predictions (41, 42) for a unitary, hydrodynamic Fermi gas.
30. A. Perali, P. Pieri, G. C. Strinati, *Phys. Rev. Lett.* **93**, 100404 (2004).
31. After the cloud expands for a time t_{heat} , the energy changes when the trapping potential $U(\mathbf{x})$ is abruptly restored, i.e., $\Delta E(t_{heat}) = \int d^3\mathbf{x}[n(\mathbf{x}, t_{heat}) - n_0(\mathbf{x})]U(\mathbf{x})$, where $n(\mathbf{x}, t_{heat})$ is the density of the expanded cloud, which is related by a scale transformation (1, 33) to the density prior to release, which takes the form of a zero temperature T-F profile $n_0(x, y, z)$ (29). Using this method, we obtain Eq. 2 as well as the anharmonic correction ΔE arising for a gaussian beam trapping potential. For a cylindrically symmetric trap: $\Delta E/E_0 = -\mu_0[2b_{\perp}^4(t) + b_{\perp}^2(t) - 3]/(30U_0) + \mu_0^2[4b_{\perp}^6(t) + 2b_{\perp}^4(t) + 3b_{\perp}^2(t) - 9]/(360U_0^2)$. Note that for our experiments, we assume a gaussian beam potential with three different dimensions.
32. N. W. Ashcroft, N. D. Mermin, *Solid State Physics* (Holt, Rinehart, and Winston, New York, 1976).
33. C. Menotti, P. Pedri, S. Stringari, *Phys. Rev. Lett.* **89**, 250402 (2002).
34. J. Stajic, Q. Chen, K. Levin, Measuring condensates in fermionic superfluids via density profiles in traps (2004). ArXiv:cond-mat/0408104.

35. B. Jackson, P. Pedri, S. Stringari, *Europhys. Lett.* **67**, 524 (2004). Our fit method is derived from ideas presented in this paper.
36. Q. Chen, J. Stajic, K. Levin, Thermodynamics of ultracold fermions in traps (2004). ArXiv:cond-mat/0411090.
37. The quoted errors in this paper are statistical only and represent one standard error.
38. T.-L. Ho, *Phys. Rev. Lett.* **92**, 090402 (2004).
39. C. A. R. S. de Melo, M. Randeria, J. R. Engelbrecht, *Phys. Rev. Lett.* **71**, 3202 (1993).
40. J. Kinnunen, M. Rodríguez, P. Törmä, *Science* **305**, 1131 (2004).
41. S. Stringari, *Europhys. Lett.* **65**, 749 (2004).
42. H. Heiselberg, *Phys. Rev. Lett.* **93**, 040402 (2004).
43. We thank K. Levin, Q. Chen, and T.-L. Ho for stimulating correspondence, and for providing physical insights on the temperature dependence of the energy. This research is supported by the Chemical Sciences, Geosciences and Biosciences Division of the Office of Basic Energy Sciences, Office of Science, U. S. Department of Energy, the Physics Divisions of the Army Research Office and the National Science Foundation, and the Fundamental Physics in Microgravity Research program of the National Aeronautics and Space Administration.

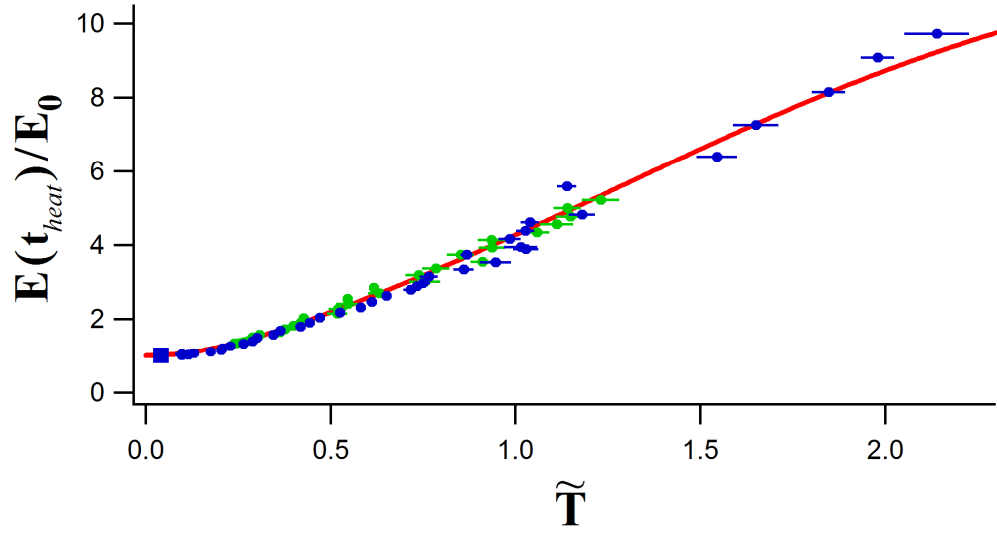


Figure 1: Total energy versus temperature. For each heating time t_{heat} , the temperature parameter \tilde{T} is measured from the cloud profile, and the total energy $E(t_{heat})$ is calculated from Eq. 2 in units of the ground state energy E_0 . Green circles: noninteracting Fermi gas data; Blue circles: strongly interacting Fermi gas data. Red curve: predicted energy versus reduced temperature for a noninteracting, trapped Fermi gas, $E_{ideal}(\tilde{T})/E_{ideal}(0)$.

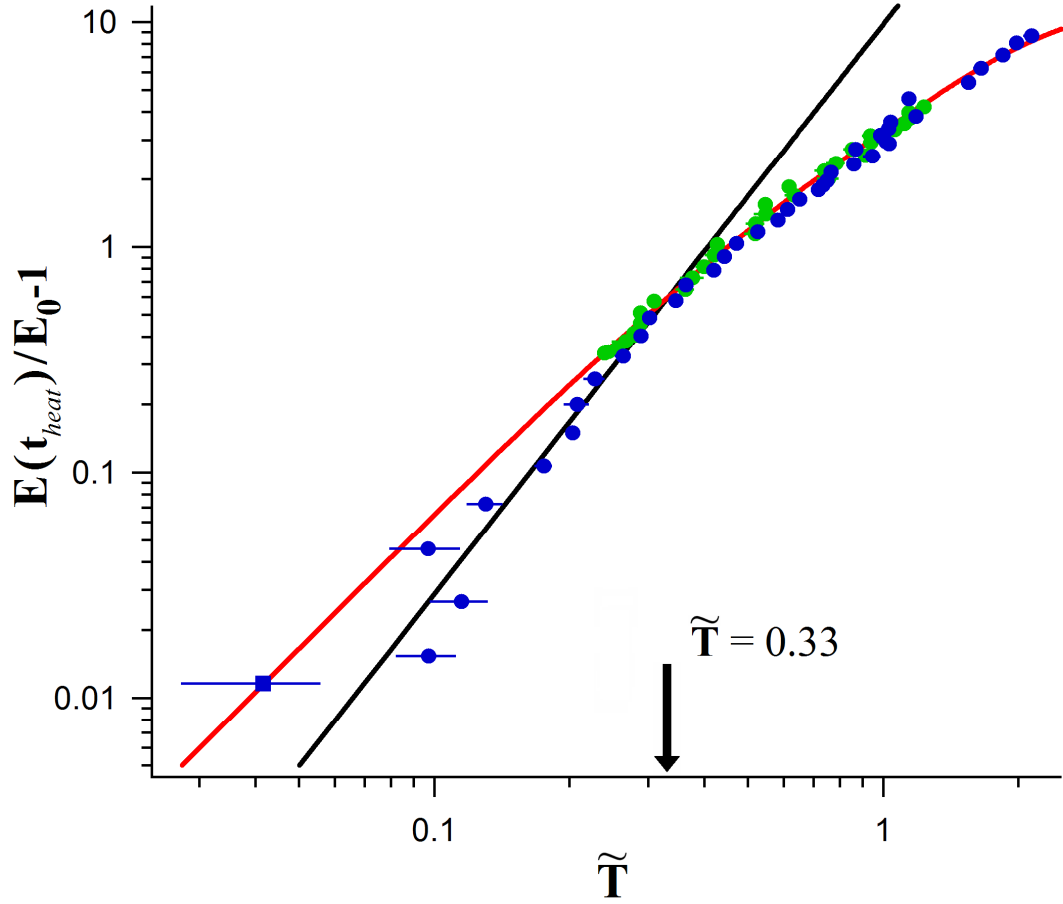


Figure 2: Energy input versus temperature from Fig. 1 on a $\log - \log$ scale. The strongly interacting Fermi gas shows a transition in behavior near $\tilde{T} = 0.33$. Green circles: noninteracting Fermi gas data; Blue circles: strongly interacting Fermi gas data. Red curve, prediction for a noninteracting, trapped Fermi gas. Black line, best fit power law $9.8\tilde{T}^{2.53}$. Note the lowest temperature point (blue square) is not included in the fits, as it is constrained to lie on the red curve.